LANGMUIR

pubs.acs.org/Langmuir Article

Interfacial Behavior of Biodegradable Poly(lactic-*co*-glycolic acid)-Pluronic F127 Nanoparticles and Its Impact on Pickering Emulsion Stability

Dániel Fülöp, Zoltán Varga, Éva Kiss, and Gergő Gyulai*

Cite This: *Langmuir* 2024, 40, 12353−12367 Read Online

ACCESS | Metrics & More | Article Recommendations | Supporting Information

ABSTRACT: Biodegradable nanoparticle-based emulsions exhibit immense potential in various applications, particularly in the pharmaceutical, cosmetic, and food industries. This study delves into the intricate interfacial behavior of Pluronic F127 modified poly(lactic-*co*-glycolic acid) (PLGA-F127) nanoparticles, a crucial determinant of their ability to stabilize Pickering emulsions. Employing a combination of Langmuir balance, surface tension, and diffusion coefficient measurements, we investigate the interfacial dynamics of PLGA-F127 nanoparticles under varying temperature and ionic strength conditions. Theoretical calculations are employed to elucidate the underlying mechanisms governing these phenomena. Our findings reveal a profound influence of temperature-dependent Pluronic layer behavior and electrostatic and steric interactions on the interfacial dynamics. Nonlinear changes in surface tension are observed, reflecting the interplay of these factors. Particle aggregation is found to be prevalent at elevated temperatures and ionic strengths, compromising the stability and emulsification efficiency of the formed emulsions. This work provides insights into the rational design of stable and efficient biodegradable nanoparticle-based Pickering emulsions, broadening their potential applications in various fields.

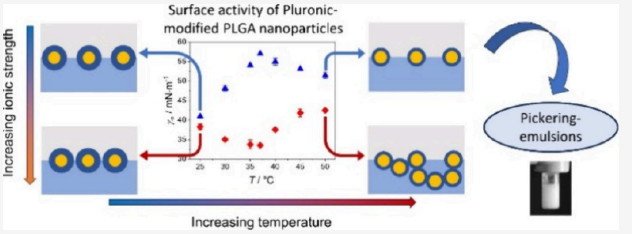

INTRODUCTION

The accumulation of nanoparticles at fluid or solid interfaces plays a crucial role in their diverse applications across various technological fields.[1] The self-assembly of particles at fluid interfaces has been extensively studied for the development of nanoporous membranes[2] and the fabrication of surface coatings with adjustable electrical, magnetic and optical properties.[3−5] The adsorption layer formed by nanoparticles at fluid interfaces has found applications in stabilizing emulsions and foams in cosmetics, pharmaceutics, and metallurgy,[6−9] as well as in mineral flotation processes.[10] Hydrophobic silica nanoparticles[11] and different types of polymeric microgels[12−14] have demonstrated significant potential as stabilizers for Pickering emulsions.

Poly(lactic-*co*-glycolic acid) (PLGA)-based systems have emerged as versatile platforms in numerous biomedical fields, including drug delivery, tissue engineering, and medical imaging, owing to their favorable biodegradability and biocompatibility.[15−18] In order to enhance their colloidal stability and biocompatibility, surface modification of these particles with poly(ethylene oxide) (PEO)-containing polymers, such as Pluronics, has been extensively explored.[19,20]

Over the past few decades, colloidal particles, such as solid particles,[21−23] fatty acid crystals,[24] microgels,[25] proteins[26,27] and polymer nanoparticles[28−33] have garnered significant interest as stabilizers for emulsions and foams. While their potential applications in the food,[21,22,26,27,34] oil well drilling,[23] and petrochemical industries[35] are well-established, their current applications as direct stabilizers in healthcare and cosmetic formulations are limited.[30] These limitations are mainly associated with the often-challenging material quality control and the difficulty to achieve adequate biocompatibility of the employed materials. PLGA nanoparticles are promising materials for such applications, due to their biodegradable and biocompatible properties. The work by Whitby et al. was the first that demonstrated this potential by successfully formulating Pickering emulsions using PVA modified PLGA nanoparticles and different oils.[32] Their findings suggest that PVA modified PLGA nanoparticles preferentially stabilize oil-in-water emulsions and the dispersion stability is determined by the combination of electrostatic and steric interactions. A subsequent study by Robin et al. has also emphasized the importance of both the particle size and hydrophobicity in optimizing the stability of Pickering emulsions.[31]

Despite extensive investigations into the properties of PLGA nanoparticles, there is still a lack of comprehensive studies dedicated to understanding their behavior at interfaces, which

Received: January 12, 2024
Revised: May 28, 2024
Accepted: May 29, 2024
Published: June 7, 2024

https://doi.org/10.1021/acs.langmuir.4c00147
Langmuir 2024, 40, 12353−12367

has a significant impact on their performance in biomedical applications. Consequently, there is a need for comprehensive interfacial studies specifically focused on PLGA nanoparticles to elucidate their interfacial properties. Such studies can aid in designing biomedical systems with enhanced stability and customizable functionalities. The work of Albert et al. exemplifies this approach.[28] Their investigation of three-phase contact angle, interfacial tension, and rheological properties of bare and PVA-modified PLGA nanoparticles at oil−water interfaces provides valuable insights into the microstructure of the prepared emulsions.

Previously, our research group conducted a detailed investigation on the interfacial behavior of bare PLGA and Pluronic-modified PLGA nanoparticles at various interfaces.[36] Building upon our previous work, the current study focuses specifically on Pluronic-modified PLGA particles at the air−water interface under different temperature conditions ranging from 25 to 50 °C. Additionally, we examine the effect of electrolytes on the interfacial properties of these nanoparticles. The primary objective of this study is to gain a deeper understanding of the structural characteristics of the interfacial films formed by Pluronic-modified PLGA nanoparticles. By employing physicochemical techniques, such as surface tension measurements, Langmuir−Blodgett trough experiments, and atomic force microscopy, we aim to unravel the interfacial organization and morphology of these nanoparticles at the air−water interface. Furthermore, we aim to find a correlation between the observed interfacial behavior and the actual capability of the particles to stabilize Pickering emulsions. By elucidating the interfacial properties and their impact on the colloidal stability of Pickering emulsions, our findings aim to contribute to the growing understanding of Pluronic-modified PLGA nanoparticles as potential stabilizers.

EXPERIMENTAL SECTION

Materials. Acid terminated poly(D,L-lactic-*co*-glycolic acid) (PLGA) with a 50% lactic and 50% glycolic content (Mw: 38,000−54,000. Inherent viscosity of 0.1% solution in $CHCl_3$ at 25 °C is 0.45−0.60 dL/g) was sourced from Sigma−Aldrich (Resomer RG 504H), Hungary. Pluronic F127, a poly(ethylene oxide)/poly(propylene oxide)/poly(ethylene oxide) triblock copolymer (M_w: 12,700), provided by BASF Hungaria Kft., was utilized for surface modification. The average composition of Pluronic F127 according to the manufacturer is 202 ethylene oxide (EO) units and 56 propylene oxide (PO) units. Cobalt(II) nitrate hexahydrate ($Co(NO_3)_2{\cdot}6H_2O$) and ammonium thiocyanate ($NH_4(SCN)$) were acquired from Sigma-Aldrich for determining the Pluronic content of nanoparticle sols via complex formation with cobalt(II) thiocyanate (CoSCN) and PEO. Branched poly(ethylene-imine) (PEI, M_w: 25,000) obtained from Sigma-Aldrich, Hungary, was employed to enhance nanoparticle adhesion to the substrates for Langmuir-film deposition.

All organic solvents used were of analytical grade. Acetone was employed for nanoparticle preparation, while dichloromethane and methanol were utilized for cleaning the Langmuir trough and its barriers. Aqueous nanoparticle sols were mixed with 2-propanol for spreading on the aqueous surface in Langmuir monolayer studies. Miglyol 812, procured from Caesar & Loretz GmbH (Germany), a pharmaceutical oil, was used for formulating Pickering-emulsions. Miglyol 812 is a blend of triglyceride esters of caprylic and capric acids.

Doubly distilled water, tested for conductivity (<5 mS) and surface tension (>72.0 mN/m at 25.0 ± 0.5 °C), served as the medium for aqueous solutions, preparation of Pickering-emulsions, and as the subphase in the Langmuir balance experiments.

Nanoparticle Formation and Characterization. Pluronic F127 modified PLGA nanoparticles (PLGA-F127) with a narrow size distribution were prepared using the nanoprecipitation method, following a previously described procedure.[36−38] In brief, PLGA was dissolved in acetone at a concentration of 10 g/L. A total of 5 mL of the organic solution was slowly added dropwise, with magnetic stirring at 500 rpm, to 50 mL 1 g/L aqueous solution of Pluronic F127 to produce the PLGA-F127 nanoparticles. During the nanoprecipitation process, Pluronic molecules form a physisorption layer on the surface of PLGA particles. Although PLGA nanoparticles have a negatively charged surface due to the chain-end carboxylic groups, their surface contains hydrophobic domains, as indicated by the water contact angle of pure PLGA, which is reported to be in the 70°−80° range.[36,39] Nejadnik et al. demonstrated that on such surfaces, Pluronic F127 forms oriented adsorption layers with a brush configuration.[40] In this arrangement, amphipathic Pluronic molecules attach to the surface via hydrophobic interactions mediated by their hydrophobic poly(propylene oxide) blocks, while the hydrophilic poly(ethylene oxide) chains orient toward the aqueous phase.[19,37] After complete acetone evaporation, the nanoparticle sols were subjected to centrifugation at 12000*g* for 20 min. The supernatant was discarded, and the pellet containing the particles was redispersed in doubly distilled water. This purification process was repeated four times until the surface tension of the supernatant exceeded 72 mN/m, indicating the removal of all unbound Pluronic. The mass concentration of the sols was determined by measuring the dry mass.

The determination of Pluronic content in PLGA-F127 nanoparticles was performed using a colorimetric method based on the formation of a precipitate between the ethylene-oxide segments of Pluronic molecules and cobalt(II) thiocyanate.[41] To prepare the cobalt(II) thiocyanate reagent, 4.8 g (16.4 mmol) of cobalt nitrate hexahydrate and 20 g (263 mmol) of ammonium thiocyanate were dissolved in 100 mL of doubly distilled water. For the analysis, 500 μL of PLGA sample with a known concentration of dry mass was mixed with 200 μL of cobalt(II) thiocyanate and 500 μL of ethyl acetate. The samples were vortexed for 1 min at 3000 rpm and then centrifuged at 12000*g* for 30 min. The resulting ethyl acetate and aqueous layers were separated, and the insoluble Pluronic complex sediment was dissolved in 1 mL of acetone. The absorbance of the solution was measured at 624 nm using a spectrophotometer. The Pluronic content of the particles was determined by comparing the absorbance to a calibration curve generated from known concentrations of Pluronic solutions using the same procedure. The used calibration curve is presented in Supplementary Figure 1.

To approximate the aqueous contact angle of the nanoparticles for modeling the interactions at the air−water interface, thin layers were prepared by casting a 500 μL acetonic solution containing 10 g/L PLGA50 and 0.5 g/L Plutonic F127 onto 2 cm × 2 cm microscopy cover glasses. The resulting films were subjected to heat treatment at 60 °C for 2 h. Prior to conducting measurements, the samples were immersed in the corresponding aqueous medium for 30 min. Contact angle measurements based on optical contour analysis were performed using an OCA25 instrument (Dataphysics, Germany) in the temperature range of 25−50 °C and with NaCl concentrations of 0, 10, 50, and 150 mM. The captured bubble method was employed for the contact angle determination.

The average hydrodynamic size and polydispersity of the PLGA nanoparticles were determined using a dynamic light scattering (DLS) system (NanoLab 3D, LSI Instruments, Switzerland). The instrument was equipped with a single model fiber detector that included integrated collimation optics and a two-channel multiple τ-correlator for auto- and cross-correlation measurements. A fiber-coupled laser-diode, operating at a wavelength of 685 nm and emitting vertically polarized light, was utilized as the light source. The DLS measurements were performed via the modulated 3D cross correlatioin mode at a detection angle of 90° within a temperature range of 25−50 °C, with a temperature accuracy of ±0.1 °C. The nanoparticle samples were diluted with doubly distilled water to 1 g/L concentration. The recorded autocorrelation functions were analyzed using the second-order cumulant expansion method. The particle sizing analysis was conducted on a minimum of three particle

https://doi.org/10.1021/acs.langmuir.4c00147
Langmuir 2024, 40, 12353−12367

preparations, and for each preparation, five parallel measurements were taken.

Nanoparticle morphology was also investigated via transmission electron microscopy. Two μL sample (2 g/L) was applied to a Formvar/Carbon 200 mesh copper grid (Ted Pella Inc., USA) and incubated for 2 min. The excess suspension was blotted with a piece of filter paper. Next, the grid was placed on a drop of 2% uranyl acetate (v/v) solution for 10 s, blotted, and then placed on a drop of water again for 10 s. After blotting the excess solution, the grid was air-dried and viewed using a MORGAGNI 268D transmission electron microscope (FEI, Eindhoven, The Netherlands) operated at 80 kV and equipped with a Quemesa 11 megapixel bottom-mounted CCD camera (Emsis GmbH, Germany).

The electrophoretic mobility of the nanoparticles was determined using a Malvern Zetasizer Nano Z apparatus within the same temperature range and 1 g/L particle concentration. The zeta potential (ζ) was calculated from the mobility values using the Smoluchowski approximation. The determined zeta potentials were used as estimates of the surface potential of the particles in the model calculations. Since the addition of electrolytes reduces the measurable zeta potential, pure water was used during the experiments. The measurements were performed in triplicate, and the obtained ζ values showed a reproducibility within $\pm$1 mV.

Langmuir Monolayer Studies. Monolayer studies of the nanoparticles (NPs) were conducted using a KSV NIMA Langmuir trough (Biolin Scientific, Sweden) (dimensions: 580 mm × 145 mm × 4 mm) equipped with two moving barriers to ensure symmetric film compression, with a maximum compression ratio of 18. The surface pressure (π), defined as the difference between the surface tension of the pure and the particle-covered surface ($\pi = \gamma_0 - \gamma$), was measured with a Wilhelmy plate made of chromatography paper (Whatman Chr1, Cytiva) connected to a force transducer, with an accuracy of 0.05 mN/m. The trough and barriers were composed of PTFE and were cleaned with dichloromethane, methanol, and water. Measurements were performed at a temperature of 25.0 ($\pm$0.5) °C, using double distilled water and a 150 mM NaCl solution as subphases.

For the preparation of Langmuir layers, the aqueous particle sol was mixed with 2-propanol in a 1:1 volume ratio. No aggregation was observed visually, and dynamic light scattering (DLS) measurements confirmed the absence of aggregates. The sample spreading process involved gradual, step-by-step dosing to minimize subphase mixing. Liquid dosing utilized a syringe fitted with a 32-gauge needle, generating small droplets at the needle tip. These droplets were delicately brought into contact with the water surface, with a waiting period of 5−10 s before further deposition. A known quantity of the sample was spread on the water subphase, allowing the particles to equilibrate and the 2-propanol to evaporate for 15 min. Surface pressure - area isotherms were recorded with three compression−expansion cycles at a barrier speed of 32 mm/min. The recorded isotherms, performed in triplicates, demonstrated remarkable reproducibility within 0.5 mN/m.

Morphology of NP Layers. The morphology of the Langmuir monolayers of PLGA-F127 NPs was investigated using atomic force microscopy (AFM). The Langmuir-Schaeffer technique was employed to transfer the surface film of particles from the Langmuir balance onto solid substrates. Microscope cover glasses (22 mm × 40 mm × 0.16 mm) were chosen as substrates and were cleaned using freshly prepared "piranha solution". To enhance particle adhesion, PEI was adsorbed from a 1 g/L aqueous solution onto the cleaned substrates. The transferred particle films were imaged at room temperature in air using a Nanosurf FlexAFM atomic force microscope (AFM) system (Nanosurf, Switzerland). Measurements were performed in dynamic mode using NSC14 cantilevers (Micromash, Estonia). Images were collected at 20−30 randomly selected locations with a typical scan area of 10 μm × 10 μm.

Adsorption Measurements. The interfacial properties of PLGA-F127 nanoparticles were investigated using an OCA 25 pendant drop tensiometer (Dataphysics, Germany) at the air−water and Miglyol 812-water interfaces. The interfacial tension of F127-PLGA nanoparticles was monitored over time in a temperature range of 25−50 °C. The concentration of nanoparticle aqueous sols was maintained at a constant value of 1.0 g/L for all experiments. Measurements were conducted with varying NaCl concentrations (0, 10, 50, and 150 mM) to examine the effect of electrolyte concentration on the adsorption of PLGA-F127 nanoparticles. To prevent water condensation during measurements at higher temperatures, the needle of the Hamilton syringe was hydrophobized using a hydrophobization kit (Dataphysics, Germany). The adsorption of nanoparticles was monitored until the difference in interfacial tensions reached a value less than 0.5 mN/m within a 10 min period. Assuming a diffusion-controlled adsorption process, the equilibrium surface tension of the sols was determined using the asymptotic solution of the Ward-Tordai equation for the t → ∞ case:

$$\gamma_{t\to\infty} = \gamma_\infty - \frac{RT\Gamma^2}{2c_0}\left(\frac{\pi}{D}\right)^{1/2} t^{-1/2} \quad (1)$$

Here, γ and γ_∞ represent the dynamic and equilibrium surface tensions, respectively. R is the universal gas constant, T is the temperature, Γ is the surface excess concentration, c_0 is the bulk concentration, and D is the diffusion coefficient. By plotting the measured surface tension as a function of $t^{-1/2}$, the value of γ_∞ can be determined as the intersection of a linear fit of the data at high t values.

The apparent diffusion coefficient (D_{eff}) of the particles was determined using the initial part of the surface tension time data. For this purpose, the $t \to 0$ case of the asymptotic approximate solution of the Ward-Tordai equation was employed, which can be expressed as

$$\gamma_{t\to 0} = \gamma_0 - 2N_A c_0 \Delta G\left(\frac{D_{\text{eff}} t}{\pi}\right)^{1/2} \quad (2)$$

Here, γ represents the interfacial tension, γ_0 is the interfacial tension of the pure interface, N_A is the Avogadro number, ΔG is the adsorption free energy of the particles (approximated based on eq 3).

Emulsion Preparation and Characterization. Miglyol 812-water emulsions were prepared using a tip sonicator (BioLogics Inc., USA) at 25, 35, and 45 °C. In a glass vial, 3 mL of the aqueous phase and 0.3 mL of the oil phase were combined and immersed into a thermostatic bath for 10 min. The aqueous phase comprised either pure water or a 1 g/L sol of PLGA-F127 nanoparticles. Emulsion preparation involved sonication of the two-phase systems for 3 min at 30 W intermittent power, with an 80% lag time. The sample temperature was verified before and after sonication. Postemulsification, the sample temperature was within 1 °C of the thermostat.

Emulsions were examined using an optical light microscope (Reichert, Austria) equipped with a 100x/1.32 objective using the immersion oil technique ($n_{D,20\,^\circ C}$ = 1.515). Images were captured with a digital camera for analysis. Droplet size distribution charts were constructed based on a minimum of 1000 droplet sizes determined from the images using ImageJ software (v1.54d, http://rsbweb.nih.gov/ij/) utilizing manual circle fitting.

Considering that PLGA nanoparticles can degrade over time in aqueous environments, their long-term storage stability might not reflect emulsion stabilization.[30] Hence, stability was characterized by centrifuging a homogeneous volume of the freshly prepared emulsion. A visually homogeneous 2 mL portion of the emulsion was separated into glass vials. After centrifugation at 2000 rpm for 2 min, the ratio of separated oil or creamy phase volumes was measured using a digital caliper.[42]

RESULTS AND DISCUSSION

Size and Zeta-Potential of PLGA Nanoparticles. Pluronic F127-stabilized PLGA50 nanoparticles were prepared using the nanoprecipitation method. The particles were then purified, and their size was characterized using dynamic light scattering (DLS) at temperatures ranging from 25 to 50 °C, as well as in the presence of different NaCl concentrations (0, 10, 50, and 150 mM). Particle concentration was kept constant

https://doi.org/10.1021/acs.langmuir.4c00147
Langmuir 2024, 40, 12353−12367

Table 1. Average Hydrodynamic Radii and Zeta-Potential of PLGA-F127 Nanoparticles as a Function of Temperature and NaCl Concentration

	r_H/nm					
c_{NaCl}/mM	25 °C	30 °C	35 °C	40 °C	45 °C	50 °C
0	77.2 ± 0.4	78 ± 0.2	77.2 ± 0.4	77.4 ± 0.6	76.6 ± 0.1	75.1 ± 0.4
10	78.8 ± 0.2	75.5 ± 0.7	75.1 ± 0.3	74.4 ± 0.1	74.5 ± 0.3	74.7 ± 0.5
50	77.2 ± 0.3	76.9 ± 0.1	77.1 ± 0.4	76.3 ± 0.1	74.7 ± 0.1	75.3 ± 0.3
150	78.0 ± 0.3	78.2 ± 0.2	77.0 ± 0.2	77.7 ± 0.5	76.7 ± 0.2	76.7 ± 0.3
	ζ/mV					
c_{NaCl}/mM	25 °C	30 °C	35 °C	40 °C	45 °C	50 °C
0	−35.3 ± 1.1	−35.6 ± 1.0	−36.0 ± 0.8	−34.1 ± 0.9	−33.7 ± 0.4	−31.0 ± 0.5

during measurements at 1 g/L. The average hydrodynamic radii of the particles were measured and are summarized in Table 1. The polydispersity indices of the particles exhibited random fluctuations within the range of 0.05−0.07, indicating a narrow size distribution. Additionally, Table 1 presents the zeta potential values of the particles in pure water medium.

The experimental findings reveal no signs of particle aggregation in the bulk phase across different temperature and ionic strength environments. A slight decrease in the measured hydrodynamic diameters was observed with increasing temperatures in all media. This observed average decrease of approximately 2 nm can be attributed to the temperature-induced contraction of the polyethylene-oxide chains in the Pluronic surface layer.[43]

The nanoparticles exhibited a significant negative zeta potential. Since the pK_a value of PLGA is 3.85[44] and the measured pH of the polymer sol at 1 g/L concentration was 4.7 carboxylic end-groups of the PLGA chains located at the particle surface are expected to be in a dissociated state resulting in a negatively charged surface. The pure PLGA nanoparticles, without a Pluronic coating were measured to have a zeta potential of −48 mV. The reduction of zeta potential in the presence of the Pluronic layer can be attributed to a screening effect, where the polymer acts as a barrier, hindering the free movement of ions, disrupting the formation of the diffuse electric double layer.[36,37,45]

Transmission electron microscopy images of dried PLGA nanoparticles are presented in Figure 1.

PLGA-F127 nanoparticles demonstrate a spherical geometry, as observed in TEM images. The number average diameter, determined from individual measurements of 200 particles, is 91 nm (±7 nm). Discrepancies between TEM and DLS measurements are anticipated; TEM sizes appear smaller due to dehydration, while DLS tends to overestimate sizes, particularly for larger nanoparticles.

Structure of PLGA-F127 Nanoparticle Surface Layers. The Langmuir-balance technique was utilized to investigate the structure and stability of interfacial layers formed by PLGA nanoparticles. The measured surface pressures can be attributed to two main components. The first component is directly correlated with the surface area occupied by the particles at the interface. The second component arises from the interactions between the particles within the layer.[46]

Figure 2 presents the isotherms of the particles recorded at 25 °C using pure water and a 150 mM NaCl solution as subphases. The system with pure water exhibited remarkable stability, showing minimal hysteresis and no significant changes during repeated compression−expansion cycles. This suggests that the particles strongly bind to the interface with sufficient

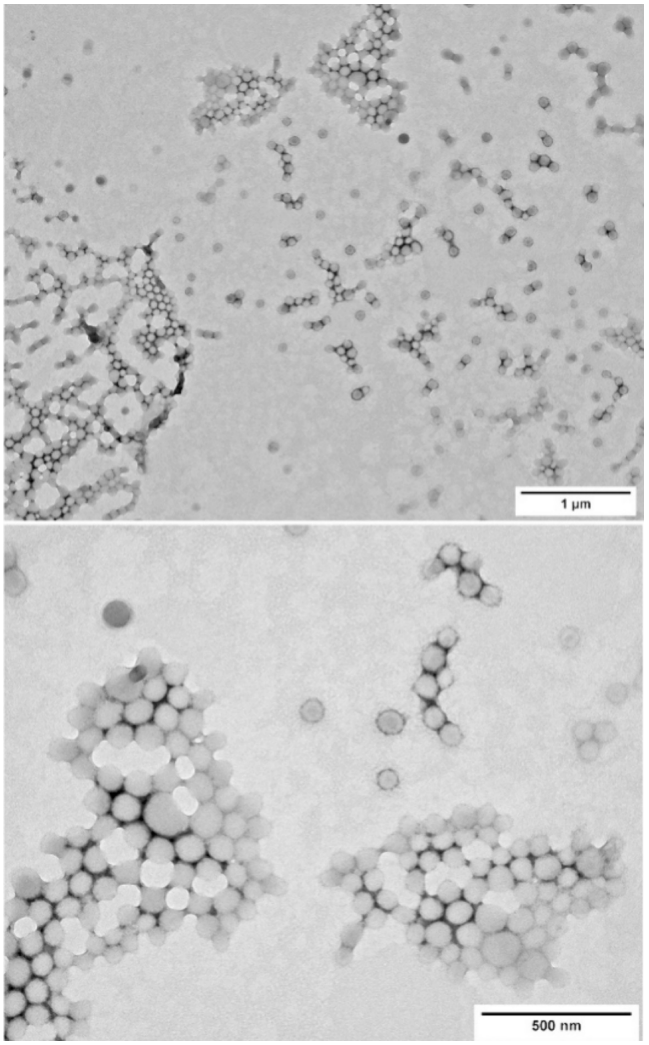

Figure 1. Transmission electron microscopy images of dried PLGA-F127 nanoparticles.

energy to prevent desorption, indicating their adsorption can be considered irreversible. This assumption is supported by the estimated free energy change (ΔG) associated with the adsorption of nanoscale objects, which can be approximated as

$$\Delta G = -r^2\pi\gamma(1 - |\cos\theta|)^2 \quad (3)$$

where r is the radius of the particle, γ is the surface tension and θ is the contact angle.[47] For the PLGA particles with an average radius of 75 nm, their binding energy significantly exceeds the available thermal energy for desorption when the

https://doi.org/10.1021/acs.langmuir.4c00147
Langmuir 2024, 40, 12353−12367

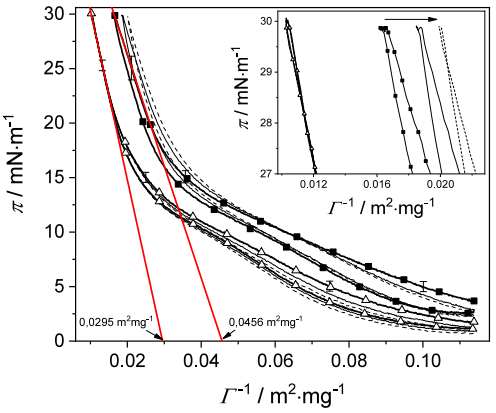

Figure 2. Successively measured isotherms of PLGA-F127 nanoparticles at air−water interfaces: (△) pure water medium, (■) 150 mM NaCl medium.

contact angle is within the range of 5−175°. Contact angles of the particles were estimated through wettability measurements on flat PLGA-Pluronic thin films, which showed slight variations with temperature and ionic strength, but no discernible tendency could be observed. The determined contact angles are presented in Supplementary Table 1. On average, a water contact angle of approximately 40° was obtained.

When the subphase contained NaCl electrolyte, significant differences were expected in the isotherm behavior. The presence of the electrolyte was anticipated to shield the electrostatic interactions between the particles, allowing for easier particle approach without invoking strong repulsive forces. Consequently, it was expected that such layers could be compressed further during the isotherm recording, reducing the effective area occupied by the particles. Contrary to these expectations, an opposite phenomenon was observed, where the particles appeared to have a higher surface area, leading to a shift in the isotherms toward increased specific surface areas at all compression states. Moreover, upon repeated compression−expansion cycles, the isotherms exhibited a further rightward shifting accompanied by a more pronounced hysteresis. To explain this contradiction, the role of the Pluronic layer on the particles should be taken into consideration. In pure water, the ethylene-oxide segments of the polymer are well-hydrated, providing the particles with a relatively hydrophilic surface and steric stability. In the presence of electrolytes, a salting-out effect may occur, reducing the polymer's hydration and diminishing its steric repulsion efficacy. The presence of hysteresis and observed isotherm shifts suggest particle aggregation during compression.[48] Formation of primary aggregates at the interface is expected to increase surface coverage inhomogeneity.[49] Upon compression, these primary aggregates form secondary loose aggregates, hindering tightly packed film formation. Additionally, Petkov et al. attribute a rightward shift in the compression isotherm to increased electrostatic repulsion among aggregates due to their combined charge.[48] Subsequent expansion cycles are likely to partially break up secondary aggregates, indicated by significant negative hysteresis, further reducing packing order in subsequent compressions.

To investigate the possible aggregation, the Langmuir films were transferred onto solid supports, and their morphology was examined using AFM. Representative AFM images showing films immobilized at a surface pressure of 25 mN/m are presented in Figure 3.

When the subphase is pure water, the particles demonstrate excellent stability, maintaining their dispersed state without significant aggregation. However, it was observed that films transferred from the electrolyte subphase displayed noticeable aggregation, providing confirmation of the results obtained from the Langmuir isotherm experiments. It is important to emphasize that this observed aggregation is primarily induced at the interface, as no aggregation could be detected in the bulk sols even at elevated temperatures and in the presence of electrolytes, as confirmed by DLS measurements.

Adsorption Kinetics of PLGA-F127 Nanoparticles. In many practical applications, interfacial particle films are formed through adsorption from the bulk phase rather than deposition. To investigate this process, interfacial adsorption studies were conducted at the aqueous-air interface, exploring different temperatures and electrolyte concentrations. The time-dependent surface tension data was utilized to calculate the equilibrium surface tension using eq 1. The surface tension's dependence on temperature and electrolyte concentration is summarized in Figure 4.

The temperature dependence of the surface tension exhibits a remarkable phenomenon between 35 and 40 °C. In the case of pure water as the medium, a significant increase in surface tension is observed from 25 °C up to 37 °C, followed by a subsequent decrease with further temperature increase. Conversely, in the presence of electrolytes, a gradual decrease in surface tension is observed up to 37 °C, followed by a significant increase in the measured equilibrium surface

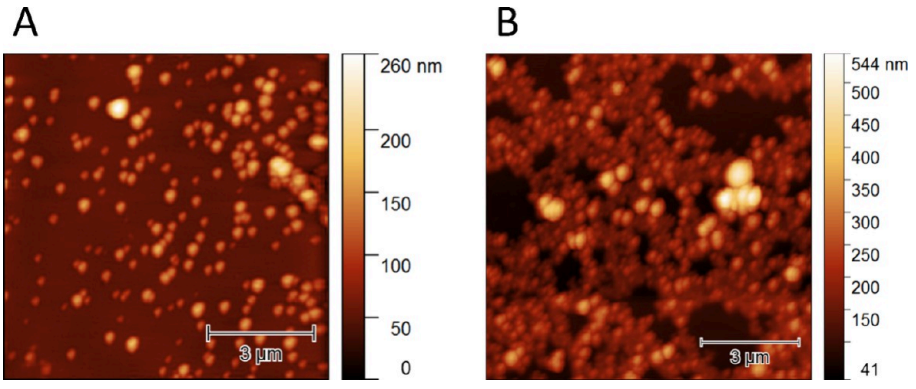

Figure 3. Morphology of particle layer at 25 °C in the presence of 0 (A) and 150 (B) mM NaCl concentration.

https://doi.org/10.1021/acs.langmuir.4c00147
Langmuir 2024, 40, 12353−12367

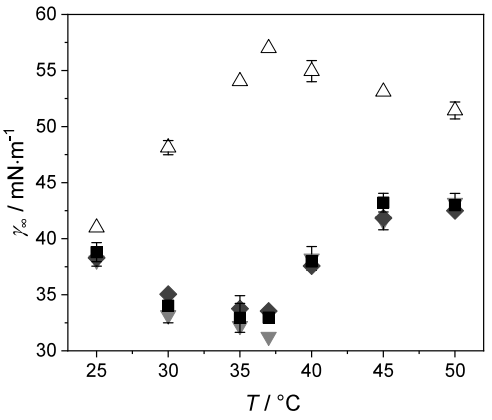

Figure 4. Temperature dependence of equilibrium surface tension values of F127-PLGA NPs at different electrolyte concentrations at air−water interfaces: (up triangle empty) pure water, (gray down triangle solid) 10 mM NaCl, (dark gray tilted square solid) 50 mM NaCl, and (black square solid) 150 mM NaCl. Error bars represent 95% confidence intervals.

tensions. This intriguing and nontrivial behavior can be attributed to structural changes occurring within the interfacial layer.

To gain a deeper understanding of the underlying processes during adsorption, the interparticle interactions were taken into account. According to the extended DLVO theory, three primary interactions occur when two particles approach each other. At close proximity, attractive van der Waals forces (U_{vdW}) come into play. Similarly charged particles experience repulsive electric double layer interactions (U_{EDL}), while at very close proximity, repulsive steric interactions (U_{St}) arise from the overlap of Pluronic surface layers. The van der Waals interactions between two spheres can be described by the equation:

$$U_{vdW} = -\frac{A_{int}}{6}\left[\frac{2r^2}{h^2+4rh} + \frac{2r^2}{(h+2r)^2} + \ln\left(1-\frac{4r^2}{(h+2r)^2}\right)\right] \quad (4)$$

Here, r represents the radius of the particles, h is the separation distance, and A_{int} is the interfacial Hamaker constant, which can be approximated using the following expression:[50,51]

$$A_{int} = (A_{11}^{1/2} - A_{22}^{1/2})^2 + \left(\frac{1-\cos\theta}{2}\right)^2 (2+\cos\theta)[(A_{11}^{1/2} - A_{33}^{1/2})^2 - (A_{11}^{1/2} - A_{22}^{1/2})^2] \quad (5)$$

In eq 5, θ represents the contact angle of the particle at the interface, and A_{11}, A_{22}, A_{33} are the Hamaker constants of PLGA, water, and air, respectively. The Hamaker constants used for the calculations were 6.5×10^{-20} J[52] for PLGA, 3.7×10^{-20} J[53] for water and 0 J for air. The measured contact angle of 40° was utilized when considering the particles at the interface. The same eq 5 can be used to calculate the van der Waals potential between particles in bulk by setting the contact angle to 0°.

The electric double layer interaction between two charged spheres can be estimated using the following equation based on the linear superposition approximation of the Poisson−Boltzmann equation using the Derjaguin approximation:[54−56]

$$U_{EDL} = 32\pi\varepsilon r f\left(\frac{k_B T}{ze}\right)^2 \tanh^2\left(\frac{ze\Psi_{NP}}{4k_B T}\right) e^{-\kappa h} \quad (6)$$

In eq 6, ε represents the dielectric permittivity of the medium, κ^{-1} is the Debye length, r and Ψ_{NP} denote the radius and surface potential of the particle, and h is the separation distance. For the calculations, the zeta potential of the particles was used as an estimated value for Ψ_{NP}. To account for the effect of the interface, a correction factor f is introduced. When $f = 1$, the equation describes the interaction between particles in bulk. However, at the interface, a decrease in repulsive forces can be expected due to the reduced dissociation of surface groups.[57] In a simplified model, only parts of the sphere that are immersed in water are considered, resulting in an f value corresponding to a simple geometric surface ratio. For particles with a contact angle of 40°, f is equal to 0.88.

The steric interaction between the particles can be approximated with the following equations:[58,59]

$$U_{St} = \tilde{\Gamma} k_B T f\left[\frac{\pi^2 L_0^2}{3h^2} - \ln\left(\frac{8\pi L_0^2}{3h^2}\right)\right] \quad \text{for} \quad h \le L_0\sqrt{3} \quad (7)$$

where h is the separation distance, L_0 is the thickness of the steric barrier polymer brush and $\tilde{\Gamma}$ is the dimensionless reduced surface coverage of the Pluronic, tha

$$U_{St} = 4\tilde{\Gamma} k_B T f \exp\left(-\frac{3h^2}{2L_0^2}\right) \quad \text{for} \quad h > L_0\sqrt{3}$$

t can be obtained as

$$\tilde{\Gamma} = \frac{\Gamma N v m}{N_A l} \quad (9)$$

In eq 9, the surface concentration (Γ) was calculated based on the molecular surface area of Pluronic on PLGA. The surface area of the Pluronic was calculated from the colorimetrically determined Pluronic content of the particles (2.1% (w/w)), resulting in an estimated value of 20 nm^2. This calculated value is in good agreement with previously published data.[60] Further parameters used in the calculation include N, the number of segments (258 for Pluronic F127); m, the average molar weight of a segment; and v, the average specific volume of the segments. The specific volumes of PEO and PPO segments were determined to be 0.84 and 0.92 cm^3/g, respectively.[61] The length of the polymeric segments (l) was considered to be the same for PEO and PPO segments, approximately 3.7 Å.[62,63] The thickness of the brush can be estimated as $L_0 \approx lN^{1/2}$, resulting in a 6 nm thickness for Pluronic F127. However, based on the DLS measurement, a small decrease of approximately 2 nm in the hydrodynamic radius was observed with increasing temperature. This could indicate a 33% decrease in the brush thickness. It is well-known that as the temperature increases, the solvation properties of water for PEO chains deteriorate, leading to a more compact conformation of the polymer and a decrease in layer thickness.[64] To account for the temperature dependence of the brush thickness, a correction factor is introduced in the calculation ($L_0 \approx alN^{1/2}$), where a linearly decreases from 1 to 0.67 as the temperature increases from 25 to 50 °C. Similarly to the U_{EDL} calculations, a correction factor (f) is introduced to consider the presence of the interface. For the bulk system, $f = 1$, while at the interface, $f = 0.88$.

https://doi.org/10.1021/acs.langmuir.4c00147
Langmuir 2024, 40, 12353−12367

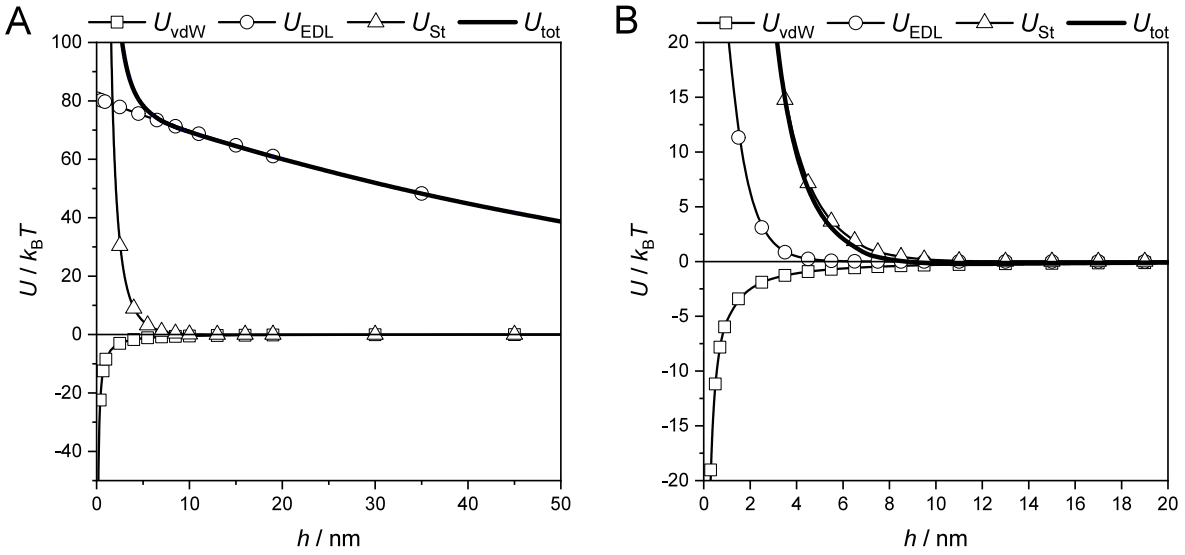

Figure 5. Representative calculated interaction energies between PLGA nanoparticle for pure water medium (A) and 150 mM NaCl medium (B) at 25 °C.

From Figure 5, it is evident that in a low ionic strength medium, the long-range interactions between particles are primarily governed by electrostatic interactions. These interactions create a substantial barrier between approaching particles, hindering their aggregation. However, as the ionic strength of the medium increases, the range of electrostatic interactions significantly decreases. Consequently, particles begin to repel each other only at very close separation distances, primarily due to steric interactions resulting from the overlap of their Pluronic surface layers.

In general, a repulsive force of $10k_BT$ is considered crucial to prevent particle collision and aggregation.[50,65] To compare the stability of different systems, the separation distance at which the total interaction energy ($U_{tot} = U_{vdW}+U_{EDL}+U_{St}$) reaches this critical value was calculated and is presented in Table 2.

Table 2. Separation Distances (h) between PLGA Nanoparticles Where the Total Repulsive Interaction Energy Reaches $10k_BT$ at Various Temperatures and Electrolyte Concentrations

	h/nm			
	Medium NaCl concentration/mM			
T/°C	0	10	50	150
25	142	6.56	4.17	3.69
30	140	6.38	3.96	3.46
35	139	6.19	3.76	3.22
40	129	5.72	3.49	2.98
45	124	5.46	3.26	2.74
50	111	4.84	2.95	2.49

In the case of a pure water medium, particles at the interface experience primarily long-distance electrostatic repulsion. The calculated values indicate that the particles are kept sufficiently separated, ensuring that their Pluronic layers do not intersect with each other.

This observation aligns with the results obtained from the Langmuir-balance isotherm measurements (Figure 2). By linearly extrapolating the steep portion of the isotherm, the effective surface area of the particles was determined. Using the calculated value of $\Gamma^{-1} = 0.0295$ m^2/mg, the effective radius of the particles was estimated to be 136 nm. Comparing this with the actual average particle radius, an average separation distance of 122 nm was found. This finding corresponds well with the theoretical separation distance at which repulsive forces become significant, preventing closer packing in equilibrium.

However, in the presence of electrolytes in the medium, a significant decrease in the separation distance is observed, indicating the effective elimination of long-range electrostatic interactions. In these cases, the main source of repulsion between particles is attributed to steric interactions. As the temperature increases, causing the Pluronic layer to become thinner, the efficiency of steric repulsion decreases. This reduction in repulsive forces, coupled with the asymmetric nature of the interface, can lead to particle aggregation.

The results of the surface tension measurements can be interpreted using the following model. In a pure water system, particles adsorb onto the interface and achieve a surface packing with significant separation distances maintained by long-range electrostatic repulsion. As the temperature increases, two simultaneous processes occur. First, a slight decrease in repulsion is calculated from the model between 25 and 35 °C, which would result in tighter packing and a decrease in surface tension. However, within this temperature range, the effect is negligible, indicating that the interparticle distance remains relatively constant. Second, as supported by the DLS measurements the Pluronic layers on the particles contract, reducing the effective diameter of the particles and limiting the number of surfactant molecules that can access the interface, leading to a decrease in measured surface activity. This means that the number of particles at the interface can be expected to remain constant while their effective coverage decreases. Overall, an increase in surface tension is observed.

Above 35 °C, the electrostatic interactions start to decrease more rapidly, as reflected by the decrease in the calculated interaction energy. This indicates that more particles can be accommodated on the interface, resulting in a tighter packing. While the Pluronic layer contraction is expected to proceed, that would further increase the surface tension, the increased

https://doi.org/10.1021/acs.langmuir.4c00147
Langmuir 2024, 40, 12353−12367

packing of nanoparticles overcomes this effect, resulting in an overall decrease in surface tension.

When electrolytes are present in the system, the role of electrostatic interactions becomes insignificant. The determined surface tension of all three systems is effectively similar. Even with 10 mM NaCl, U_{EDL} only becomes significant when the Pluronic layers are already in contact and steric interactions begin to emerge. As the temperature increases and the Pluronic layer thickness decreases, the effective area of the particles becomes smaller. Unlike in the pure water system, there are no electrostatic interactions keeping the particles apart, leading to a more tightly packed equilibrium layer and a decrease in surface tension. This decrease would be expected to continue monotonically with increasing temperature. However, above 35 °C, surface tensions start to increase. As steric interactions weaken, the likelihood of particle aggregation and flocculation increases. It is expected that particle flocculation becomes significant within this temperature range, resulting in loosely packed 3D aggregates near the interface. These aggregates hinder the formation of uniform closely packed layers, resulting in empty patches at the interface that are unavailable for adsorbing particles. This phenomenon is reflected by a decrease in apparent surface activity. A schematic illustration of the interactions and their effects on the nanoparticle configuration at the air−water interface is provided in Supplementary Figure 2.

In addition to calculating the equilibrium surface tension, the surface tension kinetics data was also utilized in determining the effective diffusion coefficients of the particles. The obtained results are depicted in Figure 6.

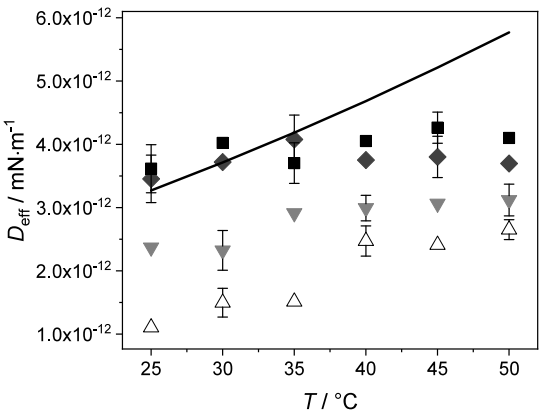

Figure 6. Effective diffusion coefficients of PLGA nanoparticles as a function of temperature and NaCl concentration: (up triangle empty) pure water, (gray triangle down solid) 10 mM NaCl, (dark gray tilted square solid) 50 mM NaCl, and (black square solid) 150 mM NaCl. Error bars represent 95% confidence intervals. The solid line represents the theoretical bulk diffusion coefficient of the particles.

The determined diffusion coefficients (D_{eff}), derived from the surface tension decrease of the system, carry information on the binding of the NPs to the interface. It is important to note that the D_{eff} values can significantly differ from the bulk diffusion coefficients, which can be determined using the Stokes−Einstein equation based on DLS data:

$$D_0 = \frac{k_B T}{6\pi\eta r} \tag{10}$$

where r is the radius of the particles and η is the viscosity of the medium. A negative deviation from the bulk diffusion coefficient suggests hindered adsorption, indicating that the attachment of particles to the interface is slowed down or prevented. In our observations, particles in pure water exhibit a significant negative deviation, suggesting substantial hindrance in their binding to the interface. However, the temperature dependence of the effective diffusion coefficients (D_{eff}) closely follows the theoretical D_0 values, indicating that the hindrance is not significantly influenced by temperature changes. Similar behavior is observed in the presence of 10 mM NaCl, although with a smaller negative deviation from D_0.

In contrast, the 50 and 150 mM NaCl media show different behavior. For these electrolytes, there are no significant changes in the determined D_{eff} values with respect to temperature up to 35 °C. Within the margin of measurement error, D_{eff} values are comparable to D_0. However, above this temperature, a negative deviation in D_{eff} is observed, suggesting a change in the binding dynamics between the interface and particles. To gain a better understanding of this behavior, further investigation into the specific interactions between the interface and the particles is required.

When particles with charges approach an interface, several types of interactions need to be considered, including van der Waals, electric double layer, and image charge interactions. These interactions can be modeled using a sphere-flat plate interaction model. The van der Waals interaction (U^*_{vdW}) between the particle and the interface can be defined using the effective Hamaker constant (A_{123}), particle radius (r), and separation distance (h):[66]

$$U^*_{vdW} = -\frac{A_{123}}{6}\left[\frac{r}{h} + \frac{r}{h+2r} + \ln\left(\frac{h}{h+2r}\right)\right] \tag{11}$$

The effective Hamaker constant (A_{123}) describing the interaction between the PLGA particle (1), air (2), and water (3) can be calculated from the bulk material Hamaker constants as

$$A_{123} = (\sqrt{A_{11}} - \sqrt{A_{33}})(\sqrt{A_{22}} - \sqrt{A_{33}}) \tag{12}$$

Image charge interactions arise when particles interact with an interface where the dielectric constants of the separated media are significantly different. The image charge (q_{im}) can be calculated based on the nominal charge of the particle (q) and the dielectric constants of the charge-containing medium (ε_1) and charge-free medium (ε_2):[67]

$$q_{im} = q\frac{\varepsilon_1 - \varepsilon_2}{\varepsilon_1 + \varepsilon_2} \tag{13}$$

In the case of water−air interface, according to eq 13 the image charge will have the same sign, since ε_1 has values in the range of 67−78, while ε_2 can be considered a constant 1. This results in repulsive image charge interactions. The image charge surface potential can be calculated by the Grahame equation as[68]

$$\Psi_{im} = \frac{2k_B T}{ze}\text{arcsinh}\left[\frac{\varepsilon_1 - \varepsilon_2}{\varepsilon_1 + \varepsilon_2}\sinh\left(\frac{ze\Psi_{NP}}{2k_B T}\right)\right] \tag{14}$$

The image charge and electric double layer interactions[55] between the particle and the interface can be given based on the linear superposition method (LSA) as

https://doi.org/10.1021/acs.langmuir.4c00147
Langmuir 2024, 40, 12353−12367

$$U_{im}^{*} = 32\pi\varepsilon r\left(\frac{k_B T}{ze}\right)^2 \tanh\left(\frac{ze\Psi_{NP}}{4k_B T}\right)\tanh\left(\frac{ze\Psi_{im}}{4k_B T}\right)e^{-2\kappa h} \quad (15)$$

$$U_{EDL}^{*} = \frac{64\pi\varepsilon}{\kappa}\left(\frac{k_B T}{ze}\right)^2 \tanh\left(\frac{ze\Psi_{NP}}{4k_B T}\right)\tanh\left(\frac{ze\Psi_{int}}{4k_B T}\right) [(\kappa r - 1)e^{-\kappa h} + (1 + \kappa r)e^{-\kappa(h+2r)}] \quad (16)$$

Where Ψ_{int}, the air−water interfacial surface potential was estimated as −15 mV.[69]

According to the DLVO theory the total interaction energy between the particle and the interface can be written as the sum of the components ($U_{tot}^{*} = U_{vdW}^{*}+U_{EDL}^{*}+U_{im}^{*}$). The separation distances at which the repulsive potential becomes $10k_B T$ are presented in Table 3.

Table 3. Separation Distances (h) between PLGA Nanoparticle and the Air−Water Interface Where the Total Repulsive Interaction Energy Reaches $10k_B T$ at Various Temperatures and Electrolyte Concentrations

	h/nm			
	Medium NaCl concentration/mM			
T/°C	0	10	50	150
25	98	7.7	4.4	3.4
30	96	7.6	4.3	3.4
35	95	7.5	4.3	3.3
40	89	7.3	4.2	3.3
45	87	7.1	4.1	3.2
50	79	6.8	4.0	3.2

If the particles are able to approach a separation distance where the Pluronic molecules on their surface come into contact with the interface, it is reasonable to expect their attachment to the interface due to the high surface activity of Pluronics. In the case of a pure water medium, the significant separation distance indicates a strong repulsive interaction between the particle surface and the interface. This barrier restricts the number of particles that can reach the interface from the bulk, resulting in slower adsorption kinetics as reflected by smaller effective diffusion coefficients (D_{eff}) than D_0.

When the medium contains 10 mM NaCl, the ionic strength is not sufficient to completely shield the electrostatic interactions. This leads to average separation distances slightly larger than the thickness of the Pluronic layer (6−4 nm), indicating hindered adsorption. However, with increased ionic strength, the energy barrier for adsorption would be localized within the Pluronic layer itself. Consequently, particles arriving from the bulk can readily adsorb onto the interface, resulting in similar effective diffusion coefficients as in the bulk solution.

The negative deviation in D_{eff} values in the case of 50 and 150 mM NaCl observed at higher temperatures can be interpreted as a sign of surface-induced aggregation, since increasing temperature would not be expected to introduce an energy barrier. Particles aggregating out of the plane are not able to reach the surface, resulting in the decrease of the apparent adsorption rate, as changes in surface tension are only recorded when new particles attach and embed into the interface.

These findings provide further support for our model of interface-induced aggregation and highlight the significance of energy barriers and interparticle interactions in determining the adsorption behavior of particles at the interface.

Having obtained insightful results from our investigations on the air−water interface, we extended our study to explore the implications of these findings in the context of emulsion stabilization. To achieve this, we conducted measurements at the Miglyol-water interface, aiming to establish a correlation between the behavior observed at the air−water interface and the stability of oil−water emulsions. The temperature-dependent interfacial tension of the PLGA-F127 sols is presented in Figure 7.

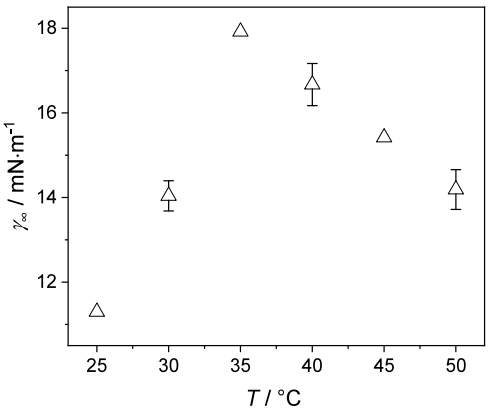

Figure 7. Tempereture dependence of equilibrium surface tension values of PLGA-F127 NPs in pure water at Miglyol 812−water interfaces.

Similar trends were observed compared to the measurements at the air−water interface (Figure 4), indicating that the processes and phenomena we observed are not limited to a specific interface but are applicable to different systems. Based on these findings, it can be concluded that the interfacial behavior of particles and the mechanisms of particle adsorption are consistent across different interfaces, such as air−water and Miglyol-water. The observed trends and phenomena provide valuable insights into the design and formulation of stable emulsions in various systems.

Pickering-Emulsion Preparation with PLGA-F127 Nanoparticles. To experimentally validate the correlation between our findings and the stability of real emulsions, we formulated emulsions of Miglyol-water with and without PLGA-F127 nanoparticles. The nature of the formed emulsion was assessed using dye tests with aqueous methylene blue solution and Sudan red in Miglyol. Based on the aqueous miscibility, an oil-in-water type emulsion formation was observed. This conforms to the Bancroft rule, indicating that the particles are readily dispersible in water but not in oils, and also consistent with the findings of Whitby et al.[32]

The droplet size of the prepared emulsions was analyzed using optical microscopy. Microscopy images of emulsions freshly prepared without the addition of electrolyte are depicted in Figure 8. Photographs of the homogeneous portion of these emulsions before and after centrifugation are also included in the figures.

The size distribution of the fresh emulsions was determined from individual drop diameter measurements obtained from microscopy images. The distribution charts are illustrated in Figure 9.

https://doi.org/10.1021/acs.langmuir.4c00147
Langmuir 2024, 40, 12353−12367

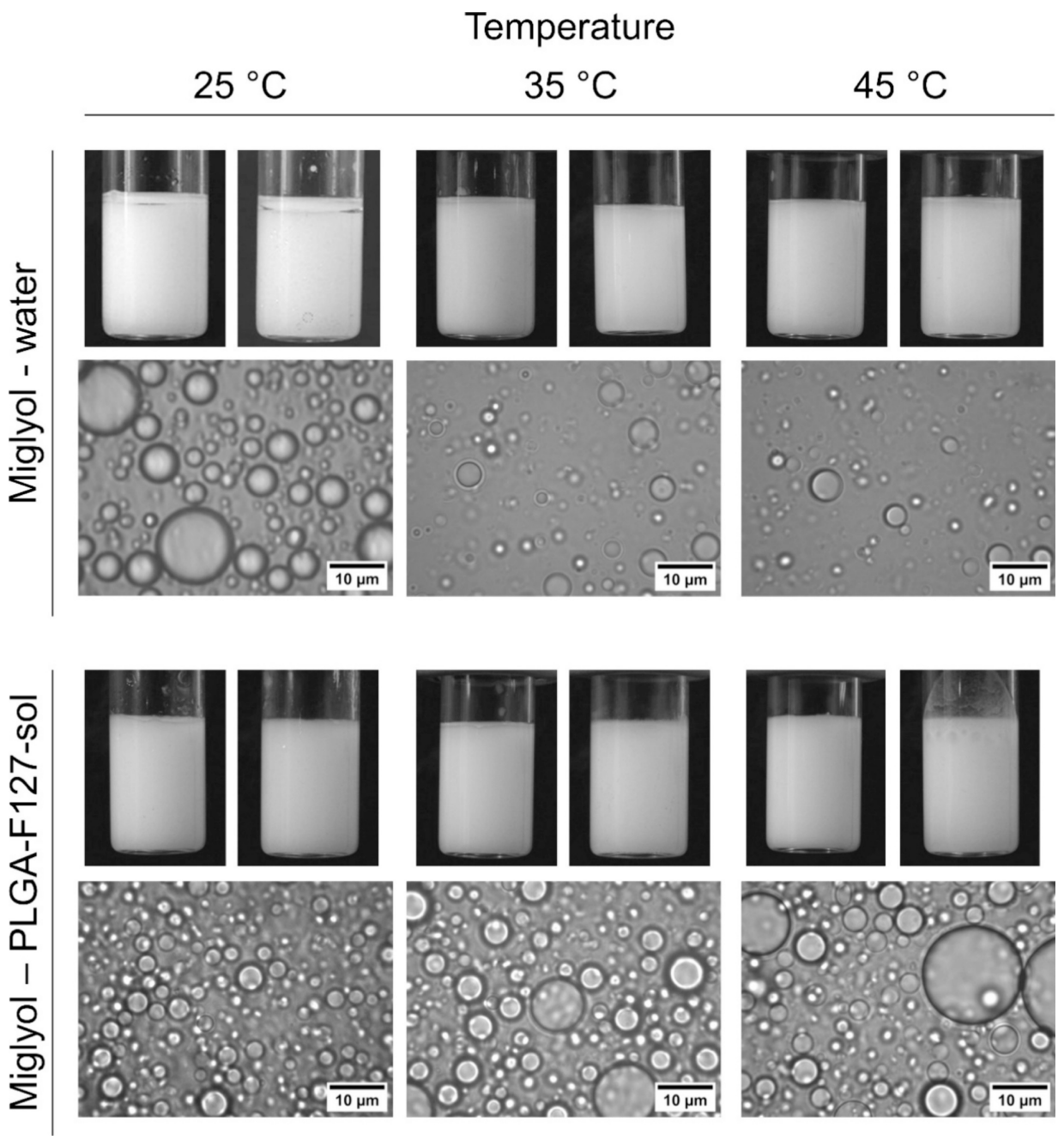

Figure 8. Photographs and microscopy images of Miglyol emulsions prepared in pure water and in PLGA-F127 aqueous sols at different temperatures. Photographs on the left show emulsions immediately after preparation, while photographs on the right depict emulsions after centrifugation.

The number-average (D_n) and volume-weighted average diameters ($D_{4,3}$) were calculated from the drop size data, and their ratio ($D_n/D_{4,3}$) was utilized to characterize the width of the size distribution. These values are summarized in Table 4, along with the phase separation volume percentage (V_S) after centrifugation.

Emulsions prepared without nanoparticles exhibited a notable presence of undispersed oil. As temperature increased, average droplet sizes decreased due to reduced liquid viscosities. Although sample polydispersity decreased and postcentrifugation separation volumes were reduced, this was primarily attributed to the decreased total dispersed oil volumes with increasing temperature, evident from the reduced number of visible droplets in microscopy images.

When preparing the emulsions with PLGA sols, no initial phase separation was observed across all temperatures. The temperature-dependent behavior seen in the emulsion size distributions aligns with our previous findings. Lower temperatures yielded more uniform droplet size distributions, indicating efficient dispersion and stabilization by nanoparticles, likely due to their ability to form stable, low-energy interfacial layers. However, broader size distributions were observed with increasing temperature. After centrifugation, although no oil phase was visible, a creamed layer formed at the vial tops, increasing in volume with higher temperatures. These results suggest that elevated temperatures enhance coalescence and reduce nanoparticle effectiveness in preventing droplet interactions and coalescence.

https://doi.org/10.1021/acs.langmuir.4c00147
Langmuir 2024, 40, 12353−12367

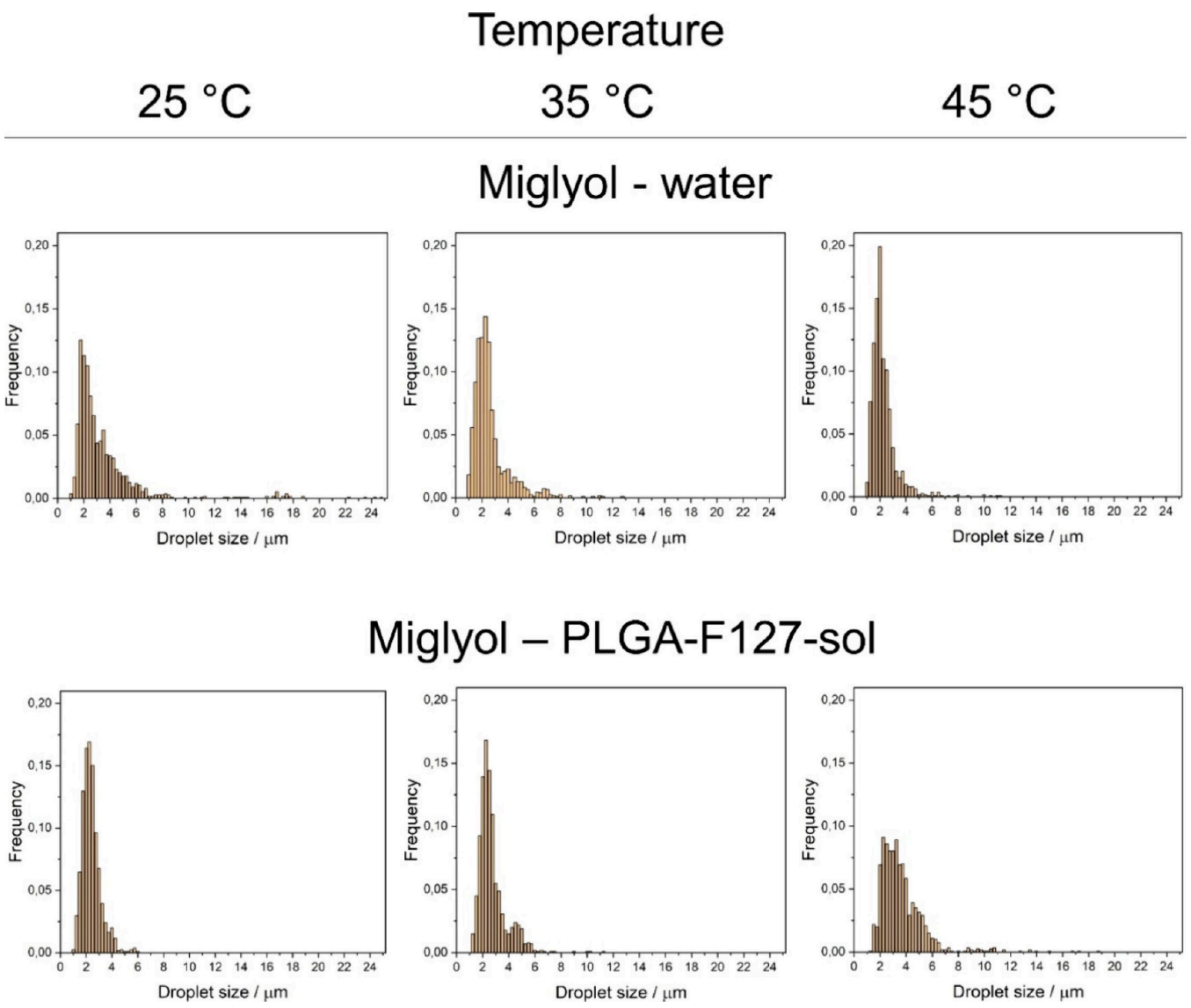

Figure 9. Size distributions of Miglyol emulsion droplets prepared in pure water and in PLGA-F127 aqueous sols at different temperatures.

Table 4. Number Average (D_n), Volume-Weighted ($D_{4,3}$) Average Droplet Sizes and Phase Separation Volume Percentage (V_S) of the Miglyol Emulsion Droplets Prepared in Pure Water and in PLGA-F127 Aqueous Sols at Different Temperatures

	T/°C	D_n/μm	$D_{4,3}$/μm	$D_n/D_{4,3}$	V_S/%
Miglyol-water	25	3,4	15,5	4,51	7,6
	35	2,6	6,1	2,33	3,9
	45	2,3	5,5	2,43	4,0
Miglyol-PLGA-F127-sol	25	2,4	3,2	1,32	3,0
	35	2,7	4,8	1,76	4,2
	45	3,6	8,6	2,37	7,2

Microscopy images were also recorded following the centrifugation, however these could not be used to meaningfully analyze the emulsion stability since following the centrifugation only the smallest droplet fractions remain in the bulk phase. These microscopy images are presented in Supplementary Figure 3.

Emulsification was also attempted in the presence of NaCl electrolyte. Already with 10 mM electrolyte concentration the emulsification efficiency was reduced significantly. Only a small amount of the oil was dispersed resulting in extremely dilute dispersions. Microscopy images and photographs are presented in Figure 10.

The presence of electrolyte hindered the formation of stable emulsions, regardless of the presence of PLGA sols. Microscopy images showed only a few polydisperse droplets, mostly adhered to the cover glass, rendering size determination meaningless. Following centrifugation, the initially opaque emulsion completely phase-separated. This aligns with our findings, suggesting that the introduction of electrolytes diminishes the ability of PLGA nanoparticles to effectively stabilize emulsion droplets, likely due to interfacial aggregation. It is assumed that the particle configuration at the oil−water interface mirrors that of the air−water interface, given the similar trends observed in surface tension measurements at both the air−water and Miglyol-water interfaces, as illustrated in Supplementary Figure 2. While interfacial aggregation does not inherently diminish emulsion stability, Sen et al. have demonstrated the possibility of spontaneous emulsification in Pluronic-silica nanoparticle systems, where the amphiphilic nature of Pluronic aids in the formation of ordered multilayers

https://doi.org/10.1021/acs.langmuir.4c00147
Langmuir 2024, 40, 12353−12367

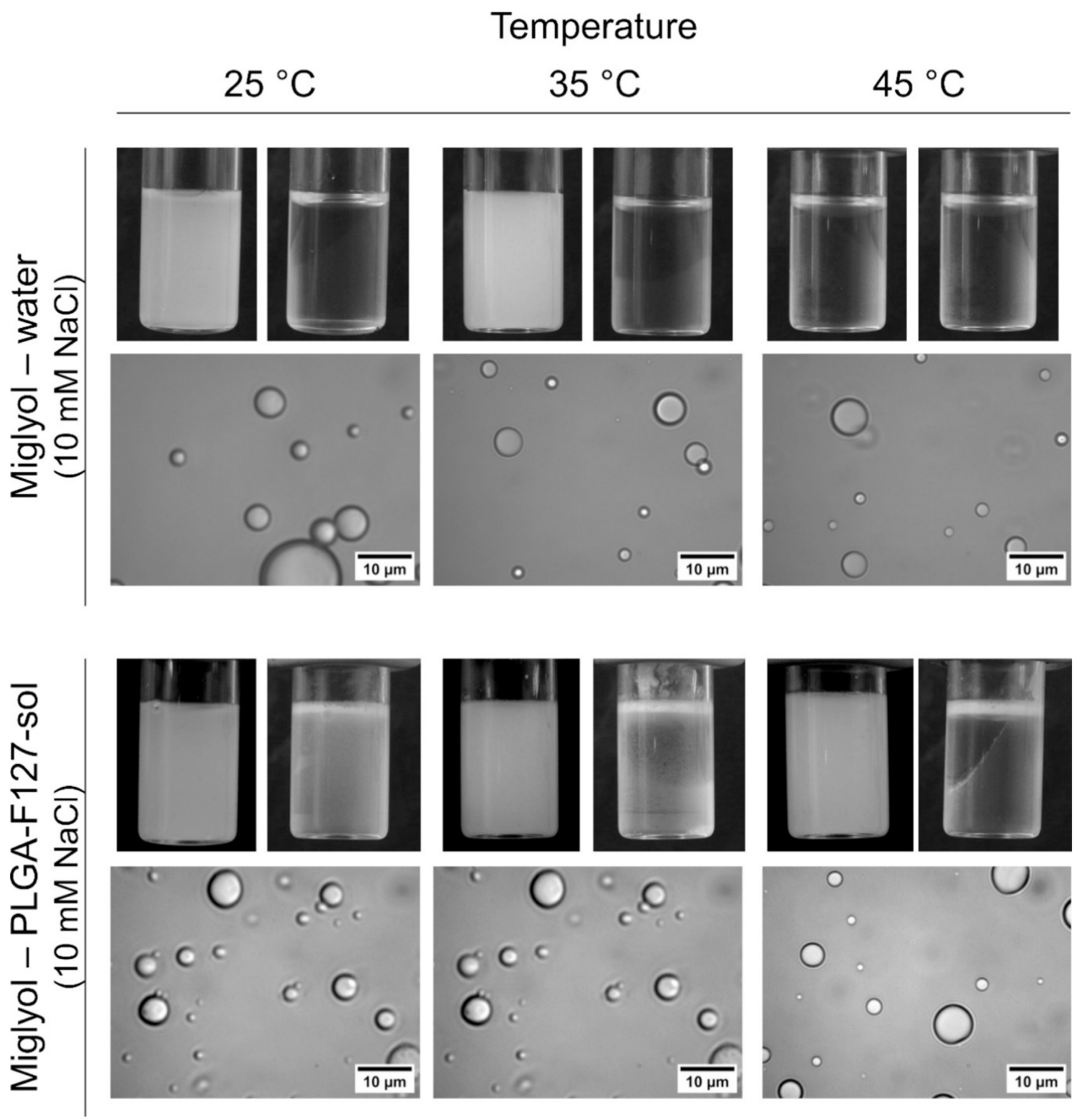

Figure 10. Photographs and microscopy images of Miglyol emulsions prepared in 10 mM NaCl solution and in PLGA-F127 + 10 mM NaCl aqueous sols at different temperatures. Photographs on the left show emulsions immediately after preparation, while photographs on the right depict emulsions after centrifugation.

around oil droplets.[70] However, in our study, the formation of loose aggregates at the interface likely results in patchy coverage of the oil droplets, promoting droplet aggregation and eventual coalescence of the oil phases through exposed contact points. Conversely, in low ionic strength environments, nanoparticles can form well-ordered monolayers around oil droplets, generating significant electrostatic repulsion upon approach and thereby enhancing emulsion stability.

CONCLUSIONS

The presented study focused on investigating the interfacial behavior of PLGA-F127 nanoparticles and its implications for emulsion stabilization. Through Langmuir-balance measurements and surface tension analyses, we gained insights into the processes occurring at the air−water interface under different temperature and ionic strength conditions. We found an unexpected nonlinear temperature dependence in the surface tension of the particle sols exhibiting a surface tension maximum in pure water and minima in the presence of electrolytes. Comparing the results with theoretical calculations, we uncovered the significant role of electrostatic and steric interactions in governing the particle arrangement and stability at the interface. Increasing the temperature results in the contraction of the Pluronic layers, reducing the steric stability and the surface activity of the individual particles, while the presence of electrolytes decreases the electrostatic interactions, allowing for increased packing densities at the

https://doi.org/10.1021/acs.langmuir.4c00147
Langmuir 2024, 40, 12353−12367

interface resulting in decreased surface tensions. However, when the temperature is elevated to a critical value in the presence of electrolytes, the close proximity of the particles, coupled with the decreased steric stability, results in surface-induced aggregation. The temperature and electrolyte concentration-dependent changes in the effective diffusion coefficients further supported the occurrence of interface-induced particle aggregation and hindered adsorption. Furthermore, we carried out emulsification experiments creating PLGA-F127 nanoparticle-stabilized Miglyol-water Pickering-emulsions, which demonstrated the correlation between the interfacial behavior of PLGA nanoparticles and the stability of emulsions. The temperature-dependent emulsion droplet size highlighted the importance of understanding the interfacial properties of nanoparticles for the rational design of Pickering-emulsions. Overall, our findings provide valuable insights for the development of biodegradable nanoparticle-based emulsions with improved stability and controlled properties.

■ ASSOCIATED CONTENT

Data Availability Statement

The raw/processed data required to reproduce these findings will be shared upon request by contacting the corresponding author.

Supporting Information

The Supporting Information is available free of charge at https://pubs.acs.org/doi/10.1021/acs.langmuir.4c00147.

Colorimetric standard curve for Pluronic F127; average water contact angles of PLGA-F127 films at various temperatures and NaCl concentrations; schematic model of interactions and particle configuration at the air−water interface; microscopy images of Miglyol emulsions prepared in pure water and in PLGA-F127 aqueous sols at different temperatures immediately after preparation and after centrifugation (PDF)

■ AUTHOR INFORMATION

Corresponding Author

Gergő Gyulai − *Laboratory of Interfaces and Nanostructures, Institute of Chemistry, Eötvös Loránd University, H-1518 Budapest, Hungary;* orcid.org/0000-0002-1352-2014; Phone: +36-1-3722500/1316; Email: gyulai.gergo@ttk.elte.hu

Authors

Dániel Fülöp − *Laboratory of Interfaces and Nanostructures, Institute of Chemistry and Hevesy György Ph.D. School of Chemistry, Eötvös Loránd University, H-1518 Budapest, Hungary*

Zoltán Varga − *Biological Nanochemistry Research Group, HUN-REN Research Centre for Natural Sciences, Institute of Materials and Environmental Chemistry, H-1117 Budapest, Hungary; Department of Physical Chemistry and Materials Science, Faculty of Chemical Technology and Biotechnology, Budapest University of Technology and Economics, H-1111 Budapest, Hungary*

Éva Kiss − *Laboratory of Interfaces and Nanostructures, Institute of Chemistry, Eötvös Loránd University, H-1518 Budapest, Hungary*

Complete contact information is available at: https://pubs.acs.org/10.1021/acs.langmuir.4c00147

Notes

The authors declare no competing financial interest.

■ ACKNOWLEDGMENTS

Financial support of National Research, Development and Innovation Office, Hungary (NKFIH Grant No. 142754) is gratefully acknowledged. Furthermore, the studies were also supported by grant (VEKOP-2.3.3-15-2017-00020 and VEKOP-2.3.2-16-2017-00014) from the European Union and the State of Hungary, cofinanced by the European Regional Development Fund. This work was partially funded by the Hungarian National Research, Development, and Innovation Office (NKFIH) grants 2020-1-1-2-PIACI-KFI_2020-00021, and TKP2021-EGA-31.

■ REFERENCES

(1) Nyström, L.; Malmsten, M. Surface-Bound Microgels — From Physicochemical Properties to Biomedical Applications. *Adv. Colloid Interface Sci.* **2016**, *238*, 88−104.

(2) Lin, Y.; Skaff, H.; Böker, A.; Dinsmore, A. D.; Emrick, T.; Russell, T. P. Ultrathin Cross-Linked Nanoparticle Membranes. *J. Am. Chem. Soc.* **2003**, *125* (42), 12690−12691.

(3) Collier, C. P.; Saykally, R. J.; Shiang, J. J.; Henrichs, S. E.; Heath, J. R. Reversible Tuning of Silver Quantum Dot Monolayers Through the Metal-Insulator Transition. *Science* **1997**, *277* (5334), 1978−1981.

(4) Detrich, Á.; Nagy, N.; Nyári, M.; Albert, E.; Zámbó, D.; Hórvölgyi, Z. Nanostructured Antireflective Bilayers: Optical Design and Preparation. *Mater. Chem. Phys.* **2014**, *145* (1−2), 176−185.

(5) Lü, T.; Zhang, S.; Qi, D.; Zhang, D.; Vance, G. F.; Zhao, H. Synthesis of pH-Sensitive and Recyclable Magnetic Nanoparticles for Efficient Separation of Emulsified Oil from Aqueous Environments. *Appl. Surf. Sci.* **2017**, *396*, 1604−1612.

(6) Nan, F.; Wu, J.; Qi, F.; Fan, Q.; Ma, G.; Ngai, T. Preparation of Uniform-Sized Colloidosomes Based on Chitosan-Coated Alginate Particles and Its Application for Oral Insulin Delivery. *J. Mater. Chem. B* **2014**, *2* (42), 7403−7409.

(7) Marku, D.; Wahlgren, M.; Rayner, M.; Sjöö, M.; Timgren, A. Characterization of Starch Pickering Emulsions for Potential Applications in Topical Formulations. *Int. J. Pharm.* **2012**, *428* (1−2), 1−7.

(8) Yi, T.; Liu, C.; Zhang, J.; Wang, F.; Wang, J.; Zhang, J. A New Drug Nanocrystal Self-Stabilized Pickering Emulsion for Oral Delivery of Silybin. *Eur. J. Pharm. Sci.* **2017**, *96*, 420−427.

(9) Babcsán, N.; Leitlmeier, D.; Banhart, J. Metal Foams—High Temperature Colloids. *Colloids Surf. Physicochem. Eng. Asp.* **2005**, *261* (1−3), 123−130.

(10) Zech, O.; Haase, M. F.; Shchukin, D. G.; Zemb, T.; Moehwald, H. Froth Flotation via Microparticle Stabilized Foams. *Colloids Surf. Physicochem. Eng. Asp.* **2012**, *413*, 2−6.

(11) Binks, B. P.; Yin, D. Pickering Emulsions Stabilized by Hydrophilic Nanoparticles: In Situ Surface Modification by Oil. *Soft Matter* **2016**, *12* (32), 6858−6867.

(12) Pinaud, F.; Geisel, K.; Massé, P.; Catargi, B.; Isa, L.; Richtering, W.; Ravaine, V.; Schmitt, V. Adsorption of Microgels at an Oil−Water Interface: Correlation between Packing and 2D Elasticity. *Soft Matter* **2014**, *10* (36), 6963−6974.

(13) Geisel, K.; Isa, L.; Richtering, W. Unraveling the 3D Localization and Deformation of Responsive Microgels at Oil/Water Interfaces: A Step Forward in Understanding Soft Emulsion Stabilizers. *Langmuir* **2012**, *28* (45), 15770−15776.

(14) Destribats, M.; Eyharts, M.; Lapeyre, V.; Sellier, E.; Varga, I.; Ravaine, V.; Schmitt, V. Impact of pNIPAM Microgel Size on Its Ability To Stabilize Pickering Emulsions. *Langmuir* **2014**, *30* (7), 1768−1777.

(15) Makadia, H. K.; Siegel, S. J. Poly Lactic-Co-Glycolic Acid (PLGA) as Biodegradable Controlled Drug Delivery Carrier. *Polymers* **2011**, *3* (3), 1377−1397.
(16) Gentile, P.; Chiono, V.; Carmagnola, I.; Hatton, P. An Overview of Poly(Lactic-Co-Glycolic) Acid (PLGA)-Based Biomaterials for Bone Tissue Engineering. *Int. J. Mol. Sci.* **2014**, *15* (3), 3640−3659.
(17) Karthick, V.; Panda, S.; Kumar, V. G.; Kumar, D.; Shrestha, L. K.; Ariga, K.; Vasanth, K.; Chinnathambi, S.; Dhas, T. S.; Suganya, K. S. U. Quercetin Loaded PLGA Microspheres Induce Apoptosis in Breast Cancer Cells. *Appl. Surf. Sci.* **2019**, *487*, 211−217.
(18) Ghitman, J.; Biru, E. I.; Stan, R.; Iovu, H. Review of Hybrid PLGA Nanoparticles: Future of Smart Drug Delivery and Theranostics Medicine. *Mater. Des.* **2020**, *193*, No. 108805.
(19) Santander-Ortega, M. J.; Jódar-Reyes, A. B.; Csaba, N.; Bastos-González, D.; Ortega-Vinuesa, J. L. Colloidal Stability of Pluronic F68-Coated PLGA Nanoparticles: A Variety of Stabilisation Mechanisms. *J. Colloid Interface Sci.* **2006**, *302* (2), 522−529.
(20) Gyulai, G.; Pénzes, Cs. B.; Mohai, M.; Lohner, T.; Petrik, P.; Kurunczi, S.; Kiss, É. Interfacial Properties of Hydrophilized Poly(Lactic-Co-Glycolic Acid) Layers with Various Thicknesses. *J. Colloid Interface Sci.* **2011**, *362* (2), 600−606.
(21) Kargar, M.; Fayazmanesh, K.; Alavi, M.; Spyropoulos, F.; Norton, I. T. Investigation into the Potential Ability of Pickering Emulsions (Food-Grade Particles) to Enhance the Oxidative Stability of Oil-in-Water Emulsions. *J. Colloid Interface Sci.* **2012**, *366* (1), 209−215.
(22) Kargar, M.; Spyropoulos, F.; Norton, I. T. The Effect of Interfacial Microstructure on the Lipid Oxidation Stability of Oil-in-Water Emulsions. *J. Colloid Interface Sci.* **2011**, *357* (2), 527−533.
(23) Sharma, T.; Velmurugan, N.; Patel, P.; Chon, B. H.; Sangwai, J. S. Use of Oil-in-Water Pickering Emulsion Stabilized by Nanoparticles in Combination With Polymer Flood for Enhanced Oil Recovery. *Pet. Sci. Technol.* **2015**, *33* (17−18), 1595−1604.
(24) Tenorio-Garcia, E.; Araiza-Calahorra, A.; Rappolt, M.; Simone, E.; Sarkar, A. Pickering Water-in-Oil Emulsions Stabilized Solely by Fat Crystals. *Adv. Mater. Interfaces* **2023**, *10* (31), No. 2300190.
(25) Brugger, B.; Rosen, B. A.; Richtering, W. Microgels as Stimuli-Responsive Stabilizers for Emulsions. *Langmuir* **2008**, *24* (21), 12202−12208.
(26) Fu, D.; Deng, S.; McClements, D. J.; Zhou, L.; Zou, L.; Yi, J.; Liu, C.; Liu, W. Encapsulation of β-Carotene in Wheat Gluten Nanoparticle-Xanthan Gum-Stabilized Pickering Emulsions: Enhancement of Carotenoid Stability and Bioaccessibility. *Food Hydrocoll* **2019**, *89*, 80−89.
(27) Galani, E.; Ly, I.; Laurichesse, E.; Schmitt, V.; Xenakis, A.; Chatzidaki, M. D. Pea and Soy Protein Stabilized Emulsions: Formulation, Structure, and Stability Studies. *Colloids Interfaces* **2023**, *7* (2), 30.
(28) Albert, C.; Huang, N.; Tsapis, N.; Geiger, S.; Rosilio, V.; Mekhloufi, G.; Chapron, D.; Robin, B.; Beladjine, M.; Nicolas, V.; Fattal, E.; Agnely, F. Bare and Sterically Stabilized PLGA Nanoparticles for the Stabilization of Pickering Emulsions. *Langmuir* **2018**, *34* (46), 13935−13945.
(29) Binks, B. P.; Lumsdon, S. O. Pickering Emulsions Stabilized by Monodisperse Latex Particles: Effects of Particle Size. *Langmuir* **2001**, *17* (15), 4540−4547.
(30) Qi, F.; Wu, J.; Sun, G.; Nan, F.; Ngai, T.; Ma, G. Systematic Studies of Pickering Emulsions Stabilized by Uniform-Sized PLGA Particles: Preparation and Stabilization Mechanism. *J. Mater. Chem. B* **2014**, *2* (43), 7605−7611.
(31) Robin, B.; Albert, C.; Beladjine, M.; Legrand, F.-X.; Geiger, S.; Moine, L.; Nicolas, V.; Canette, A.; Trichet, M.; Tsapis, N.; Agnely, F.; Huang, N. Tuning Morphology of Pickering Emulsions Stabilised by Biodegradable PLGA Nanoparticles: How PLGA Characteristics Influence Emulsion Properties. *J. Colloid Interface Sci.* **2021**, *595*, 202−211.
(32) Whitby, C. P.; Lim, L. H.; Ghouchi Eskandar, N.; Simovic, S.; Prestidge, C. A. Poly(Lactic-Co-Glycolic Acid) as a Particulate Emulsifier. *J. Colloid Interface Sci.* **2012**, *375* (1), 142−147.
(33) Zheng, R.; Binks, B. P. Pickering Emulsions Stabilized by Polystyrene Particles Possessing Different Surface Groups. *Langmuir* **2022**, *38* (3), 1079−1089.
(34) Yao, L.; Wang, Y.; He, Y.; Wei, P.; Li, C.; Xiong, X. Pickering Emulsions Stabilized by Conjugated Zein-Soybean Polysaccharides Nanoparticles: Fabrication, Characterization and Functional Performance. *Polymers* **2023**, *15* (23), 4474.
(35) Umar, A. A.; Saaid, I. B. M.; Sulaimon, A. A.; Pilus, R. B. M. A Review of Petroleum Emulsions and Recent Progress on Water-in-Crude Oil Emulsions Stabilized by Natural Surfactants and Solids. *J. Pet. Sci. Eng.* **2018**, *165*, 673−690.
(36) Gyulai, G.; Kiss, É. Interaction of Poly(Lactic-Co-Glycolic Acid) Nanoparticles at Fluid Interfaces. *J. Colloid Interface Sci.* **2017**, *500*, 9−19.
(37) Gyulai, G.; Pénzes, Cs. B.; Mohai, M.; Csempesz, F.; Kiss, É. Influence of Surface Properties of Polymeric Nanoparticles on Their Membrane Affinity. *Eur. Polym. J.* **2013**, *49* (9), 2495−2503.
(38) Gyulai, G.; Magyar, A.; Rohonczy, J.; Orosz, J.; Yamasaki, M.; Bősze, S.; Kiss, É. Preparation and characterization of cationic Pluronic for surface modification and functionalization of polymeric drug delivery nanoparticles. *Express Polym. Lett.* **2016**, *10* (3), 216.
(39) Kiss, É.; Takács, M. G.; Bertóti, I.; Vargha-Butler, E. I. Surface Properties of Poly(Lactic/Glycolic Acid)−Pluronic® Blend Films. *Polym. Adv. Technol.* **2003**, *14* (11−12), 839−846.
(40) Nejadnik, M. R.; Olsson, A. L. J.; Sharma, P. K.; Van Der Mei, H. C.; Norde, W.; Busscher, H. J. Adsorption of Pluronic F-127 on Surfaces with Different Hydrophobicities Probed by Quartz Crystal Microbalance with Dissipation. *Langmuir* **2009**, *25* (11), 6245−6249.
(41) Ghebeh, H.; Handa-Corrigan, A.; Butler, M. Development of an Assay for the Measurement of the Surfactant Pluronic F-68 in Mammalian Cell Culture Medium. *Anal. Biochem.* **1998**, *262* (1), 39−44.
(42) Kalashnikova, I.; Bizot, H.; Bertoncini, P.; Cathala, B.; Capron, I. Cellulosic Nanorods of Various Aspect Ratios for Oil in Water Pickering Emulsions. *Soft Matter* **2013**, *9* (3), 952−959.
(43) Zámbó, D.; Radnóczi, G. Z.; Deák, A. Preparation of Compact Nanoparticle Clusters from Polyethylene Glycol-Coated Gold Nanoparticles by Fine-Tuning Colloidal Interactions. *Langmuir* **2015**, *31* (9), 2662−2668.
(44) Yoo, J.-W.; Mitragotri, S. Polymer Particles That Switch Shape in Response to a Stimulus. *Proc. Natl. Acad. Sci. U. S. A.* **2010**, *107* (25), 11205−11210.
(45) Kumar, S.; Ganguly, R.; Nath, S.; Aswal, V. K. Pluronic Induced Interparticle Attraction and Re-Entrant Liquid−Liquid Phase Separation in Charged Silica Nanoparticle Suspensions. *Langmuir* **2023**, *39* (23), 8109−8119.
(46) Fainerman, V. B.; Kovalchuk, V. I.; Lucassen-Reynders, E. H.; Grigoriev, D. O.; Ferri, J. K.; Leser, M. E.; Michel, M.; Miller, R.; Möhwald, H. Surface-Pressure Isotherms of Monolayers Formed by Microsize and Nanosize Particles. *Langmuir* **2006**, *22* (4), 1701−1705.
(47) Hórvölgyi, Z.; Németh, S.; Fendler, J. H. Monoparticulate Layers of Silanized Glass Spheres at the Water−Air Interface: Particle−Particle and Particle−Subphase Interactions. *Langmuir* **1996**, *12* (4), 997−1004.
(48) Petkov, P. V.; Danov, K. D.; Kralchevsky, P. A. Monolayers of Charged Particles in a Langmuir Trough: Could Particle Aggregation Increase the Surface Pressure? *J. Colloid Interface Sci.* **2016**, *462*, 223−234.
(49) Vincze, A.; Agod, A.; Kertész, J.; Zrínyi, M.; Hórvölgyi, Z. Aggregation Kinetics in Two Dimensions: Real Experiments and Computer Simulations. *J. Chem. Phys.* **2001**, *114* (1), 520−529.
(50) Williams, D. F.; Berg, J. C. The Aggregation of Colloidal Particles at the Air—Water Interface. *J. Colloid Interface Sci.* **1992**, *152* (1), 218−229.

https://doi.org/10.1021/acs.langmuir.4c00147
Langmuir 2024, 40, 12353−12367

(51) Garbin, V.; Crocker, J. C.; Stebe, K. J. Nanoparticles at Fluid Interfaces: Exploiting Capping Ligands to Control Adsorption, Stability and Dynamics. *J. Colloid Interface Sci.* **2012**, *387* (1), 1−11.
(52) Chen, J.; Lee, M. K.; Qin, E.; Misra, S.; Kong, H. Van Der Waals Force-Induced Loading of Proangiogenic Nanoparticles on Microbubbles for Enhanced Neovascularization. *Nanoscale* **2015**, *7* (40), 17139−17147.
(53) Hunter, R. J. *Foundations of Colloid Science*, 2nd ed..; Oxford University Press: Oxford; New York, 2001.
(54) Bell, G. M.; Levine, S.; McCartney, L. N. Approximate Methods of Determining the Double-Layer Free Energy of Interaction between Two Charged Colloidal Spheres. *J. Colloid Interface Sci.* **1970**, *33* (3), 335−359.
(55) Lin, S.; Wiesner, M. R. Exact Analytical Expressions for the Potential of Electrical Double Layer Interactions for a Sphere−Plate System. *Langmuir* **2010**, *26* (22), 16638−16641.
(56) Gregory, J. Interaction of Unequal Double Layers at Constant Charge. *J. Colloid Interface Sci.* **1975**, *51* (1), 44−51.
(57) Girotto, M.; dos Santos, A. P.; Levin, Y. Interaction of Charged Colloidal Particles at the Air-Water Interface. *J. Phys. Chem. B* **2016**, *120* (26), 5817−5822.
(58) Dolan, A. K.; Edwards, W. F. The Effect of Excluded Volume on Polymer Dispersant Action. *Proc. R. Soc. London Math. Phys. Sci.* **1975**, *343* (1635), 427−442.
(59) Kralchevsky, P. A.; Nagayama, K. *Particles at Fluids Interfaces and Membranes: Attachment of Colloid Particles and Proteins to Interfaces and Formation of Two-Dimensional Arrays*; Studies in interface science; Elsevier: Amsterdam; New York, 2001.
(60) Kiss, É.; Gyulai, G.; Pénzes, Cs. B.; Idei, M.; Horváti, K.; Bacsa, B.; Bősze, Sz. Tuneable Surface Modification of PLGA Nanoparticles Carrying New Antitubercular Drug Candidate. *Colloids Surf. Physicochem. Eng. Asp.* **2014**, *458*, 178−186.
(61) Sommer, C.; Pedersen, J. S.; Stein, P. C. Apparent Specific Volume Measurements of Poly(Ethylene Oxide), Poly(Butylene Oxide), Poly(Propylene Oxide), and Octadecyl Chains in the Micellar State as a Function of Temperature. *J. Phys. Chem. B* **2004**, *108* (20), 6242−6249.
(62) Lee, H.; Venable, R. M.; MacKerell, A. D.; Pastor, R. W. Molecular Dynamics Studies of Polyethylene Oxide and Polyethylene Glycol: Hydrodynamic Radius and Shape Anisotropy. *Biophys. J.* **2008**, *95* (4), 1590−1599.
(63) Kiss, É.; Dravetzky, K.; Hill, K.; Kutnyánszky, E.; Varga, A. Protein Interaction with a Pluronic-Modified Poly(Lactic Acid) Langmuir Monolayer. *J. Colloid Interface Sci.* **2008**, *325* (2), 337−345.
(64) Backmann, N.; Kappeler, N.; Braun, T.; Huber, F.; Lang, H.-P.; Gerber, C.; Lim, R. Y. H. Sensing Surface PEGylation with Microcantilevers. *Beilstein J. Nanotechnol.* **2010**, *1* (1), 3−13.
(65) Shrestha, S.; Wang, B.; Dutta, P. Nanoparticle Processing: Understanding and Controlling Aggregation. *Adv. Colloid Interface Sci.* **2020**, *279*, No. 102162.
(66) Bhattacharjee, S.; Elimelech, M. Surface Element Integration: A Novel Technique for Evaluation of DLVO Interaction between a Particle and a Flat Plate. *J. Colloid Interface Sci.* **1997**, *193* (2), 273−285.
(67) Wang, H.; Singh, V.; Behrens, S. H. Image Charge Effects on the Formation of Pickering Emulsions. *J. Phys. Chem. Lett.* **2012**, *3* (20), 2986−2990.
(68) Israelachvili, J. N. *Intermolecular and Surface Forces*, 3rd ed.; Academic Press: Burlington, MA, 2011.
(69) Cho, S.-H.; Kim, J.-Y.; Chun, J.-H.; Kim, J.-D. Ultrasonic Formation of Nanobubbles and Their Zeta-Potentials in Aqueous Electrolyte and Surfactant Solutions. *Colloids Surf. Physicochem. Eng. Asp.* **2005**, *269* (1), 28−34.
(70) Sen, D.; Das, A.; Kumar, A.; Bahadur, J.; Chaurasia, R. K.; Khan, A.; Ganguly, R. Amphiphilic Interaction-Mediated Ordering of Nanoparticles in Pickering Emulsion Droplets. *Soft Matter* **2023**, *19* (21), 3953−3965.

https://doi.org/10.1021/acs.langmuir.4c00147
Langmuir 2024, 40, 12353−12367